# Analysis of the Antenna Pointing Instability of a Satellite in Spin-Stabilized Injection Mode

**Ja-Young Kang and Kwang-Keun Shin**

CONTENTS



ABSTRACT

A new mathematical model to predict the beam pointing instability of a nonconservative two-body satellite system in spinning injection mode has been developed by using Newton-Euler and projection methods. Since the on-axis and null axis of the omni antenna with toroidal pattern beam form a right angle, wobbling of the antenna on-axis is measured by determining the Euler angles which represent the orientation of the satellite's spin axis. Because of the complexity of the system which is a time varying, nonstationary, nonlinear dynamical system, a numerical method is used for the analysis. Computer simulation results present the effects of the mass distribution and internal mass motion on the antenna beam pointing.

## NOMENCLATURE

$a$ = magnitude of the lateral angular momentum

$\underline{a}_c$ = acceleration of the center of mass (c.m.) of the system

$\underline{a}_2$ = acceleration of the pendulum mass point

$C$-$xyz$ = coordinate system with origin at the c.m.

$C_1$-$x_1y_1z_1$ = body fixed centroidal principal coordinate system when the rigid configuration is maintained.

$E$-$XYZ$ = earth centered inertial reference frame

$\underline{e}_l$ = unit vector of $\underline{l}$

$\underline{e}_r$ = a vector of $\underline{r}_p$ normalized by $l$

$\underline{F}$ = $(0\ 0\ F_3)^T$ = thrusting force

$GEO$ = Geostationary Earth Orbit

$\underline{H}$ = $(H_1\ H_2\ H_3)^T$ = total angular momentum

$\underline{h}$ = $(h_1\ h_2\ h_3)^T$ = angular momentum due to disturbance mass

$[I]$ = inertia dyadic of the spacecraft body

$I_1, I_2, I_3$ = principal moments of inertia(MOI)

$[J]$ = $[I] - \mu m_1 \tilde{\underline{r}}_p \tilde{\underline{r}}_p$

$\underline{l}$ = pendulum length vector

$m_1$ = mass of the main body of the spacecraft

$m_2$ = internal disturbance mass

$n$ = initial spin rate

$P$ = projection matrix

$\underline{r}_o$ = distance vector from the c.m. to the pendulum hinge point

$\underline{r}_p$ = distance vector from the c.m. to the pendulum mass point

$\underline{T}$ = $(T_1\ T_2\ T_3)^T$ = torque due to thrusting force

$\underline{T}_o$ = $(T_{o1}\ T_{o2}\ T_{o3})^T$ = torque acting on the pendulum hinge point

$TT\&C$ = Tracking, Telemetry and Command

$t$ = time

$\alpha, \beta$ = pendulum angular displacements

$\gamma$ = ratio of the first axis MOI to the spin axis MOI

$\mu$ = ratio of the disturbance mass to the total mass of the system

$\Psi, \Theta, \Phi$ = classical Euler angles in a 3-1-3 rotation sequence

$\xi$ = $x$-axis component of the antenna depointing

$\eta$ = $y$-axis component of the antenna depointing

$\underline{\omega}$ = $(\omega_1\ \omega_2\ \omega_3)^T$ = angular velocity of the main body

## SUPERSCRIPTS & SUBSCRIPTS

$\sim$ = cross product operation on a vector

$\cdot$ = time derivative

1 = $x_1$-axis

2 = $y_1$-axis

3 = $z_1$-axis

$o$ = pendulum hinge point

$p$ = pendulum mass point

# I. INTRODUCTION

The antenna beam pointing accuracy of a satellite in the transfer orbit or in the mission orbit has been of concern to the ground operators, manufacturers and users of communications satellites for number of years.

The design of TT&C antenna is largely dictated by transfer orbit operations. To ascertain that the satellite has survived the rough ride into space, and to prepare attitude as well as orbital maneuvers, spacecraft controllers need rapid access to telemetry and ranging data. TT&C operations are virtually excluded near the perigee where satellite ground contact tends to be very brief due to the high orbital speed and low altitude of the spacecraft. Consequently, most maneuvers must be prepared and executed closer to the apogee. This coverage limitation imposes a severe time pressure on the spacecraft controllers, and it is therefore essential that they have continuous TT&C access to the satellite for as long as it is in view of the ground stations.

Because the satellite in the transfer orbit is rotating while moving across the sky and also keeps changing its attitude, the station-to-satellite vector moves through all the quadrants of the satellite's geometrical reference frame. Consequently, when the spacecraft in the transfer orbit is spinning, commands should be received via the toroidal beam omni antenna. Since the null axis of the toroidal beam antenna is parallel to the spin axis, the attitude instability (nutation) of the satellite will cause antenna depointing and, in case which it is out of bounds, communication degradation may occur. Because the antenna is fixed on the spacecraft body, the attitude of the satellite affects directly the TT&C antenna beam pointing accuracy.

Usually, nutation of a spinning spacecraft is caused by a single asymmetric impulse due to, for example, separation spring imbalance, rocket motor tailoff, motor side forces, thrust vector misalignment, or principal axis misalignment. Most causes can be minimized or eliminated in design and manufacturing processes. However, if the spacecraft does not maintain its rigid configuration during maneuver, i.e., if it has an internal moving part such as flexible structure or sloshing liquid, the nutational motion occurs and causes antenna depointing. The nutation instability of the spinning spacecraft carrying the internal moving parts has not been explained well.

Mingori and Yam [1] developed linear stability conditions for a spacecraft consisting of a symmetric rigid body and a planar pendulum, to present the sloshing mass. In their model, the pendulum mass is attached to its pivot by a spring and is free to rotate about the symmetry axis of the spacecraft. Assuming that the spacecraft is in a state of steady spin about its symmetry axis, they obtained linear equations and showed the possibility for unstable coning growth if the thrust magnitude is sufficiently large and the moving mass is aft of the system mass center. In any case, the developed stabil-

ity criteria are, in author's judgment, not applicable to nonlinear systems such as the spinning powered spacecraft with internal sloshing mass. Since the equations of motion were derived using constant parameters, the model fails to predict the dynamic behavior of the actual system whose physical parameters vary widely with time.

Or [2] also carried out a linear analysis of the stability of a spinning, thrusting spacecraft in a manner similar to that used by Mingori and Yam. To model the liquid pool, he used two types of pendulum models, one being a spherical pendulum model, the other model consisting of two orthogonal plane pendulums. His results showed that both model will produce an unstable motion if "tuned pendulum conditions" are used. The conditions he used are, however, unrealistic, since matching simulated results with flight data using his model requires a pendulum length and pivot location which places the pendulum mass outside the spacecraft. Another drawback of his model is that large amplitude motion of the linear pendulum occurs in contradiction to the assumption of linear motion. This is thought to be due to the fact that his linear equations were obtained by expanding about the vertical equilibrium condition of the pendulum. Apparently, the vertical orientation of the spinning pendulum is always statically unstable.

Cochran and Kang [3], and Kang et al. [4]-[6] have obtained significant results for describing the attitude motion of the spin-stabilized thrusting spacecraft by using the full nonlinear mathematical models to complement earlier research by others based on linearized pendulum models. By treating the motion of liquid as a perturbation of the motion of the spacecraft as a whole, they obtained nonlinear equations including viscous effects.

In the present work, based on the nonlinear liquid disturbance theory by Cochran and Kang [3], a complete set of the mathematical models to characterize the depointing mechanism of the toroidal beam omni antenna is developed and the interrelationship between the pointing instability and the system parameters such as the body configurations, mass variations and energy input due to thrusting is investigated. In the following two sections, the physical and mathematical modeling procedures are described and definitions for the used coordinates systems are given. In Section IV, extensive computer simulations are conducted for three basic satellite configurations. In the conclusion section, the results of the study are summarized and solutions for eliminating the pointing instability are suggested.

## II. DESCRIPTION OF THE PHYSICAL MODEL

Fig. 1 shows transition of the satellite from the parking orbit through the geosynchronous transfer orbit to the geostationary orbit using a perigee kick motor and an apogee kick motor after release from the orbiter.

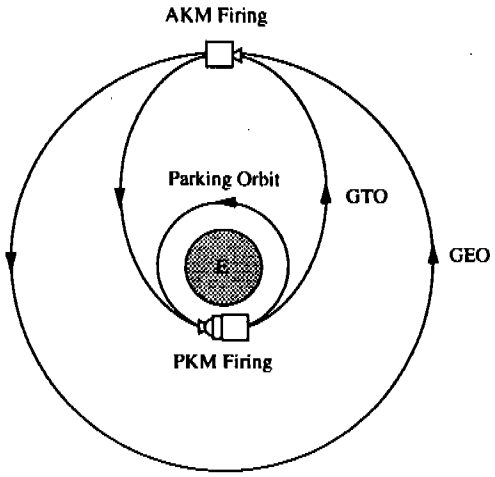


Fig. 1. Orbit transfer of a satellite from the earth to the GEO.

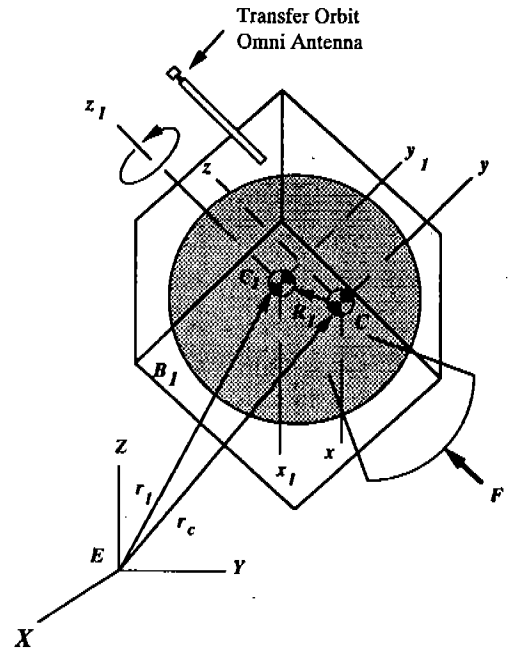


Fig. 2. Satellite in the inertial frame.

In Fig. 2 is shown a schematic diagram of the satellite to be used as a physical model for the present study. The coordinate system $E$-$XYZ$ is the earth centered inertial reference frame, $C$-$xyz$ is a coordinate system with origin at the center of mass of the system, and the $C_1$-$x_1y_1z_1$ is a body fixed centroidal principal coordinate system when the rigid configuration is maintained. The coordinate system $C$-$xyz$ is the new centroidal but not principal coordinate system after mass change.

Fig. 3 represents the basic geometric description of the satellite system to be used for analysis. The asymmetric satellite is modeled as a variable-mass rigid body with center of mass $C_1$ and axes $x_1$, $y_1$ and $z_1$ which do not rotate with respect to the body. The liquid is modeled as a point mass which is "encouraged" to move on a wall at the base of the body by including a rigid string at the pendulum pivot point [7]. Motion of the pendulum is described geometrically by the two angles $\alpha$ and $\beta$. The angle $\beta$ is unconstrained, but a viscous torque proportional to $\dot{\beta}$ tends to make the pendulum bob rotate with the body. The TT&C antenna (transfer orbit omni antenna) is mounted on the body-fixed pole which is parallel to but off the spin axis ($z_1$ axis). Therefore, there is no relative motion between the antenna and satellite body. The rigid body, $B_1$, has mass $m_1$ with centroidal, principal mass moments of inertia, $I_1$, $I_2$, $I_3$, about the axes $x_1$, $y_1$ and $z_1$ respectively, and center of mass, $C_1$. The mass and

moments of inertia of $B_1$ change with time, but the only direct, significant cause of the time rate of change of the mass $m_1$ is assumed to be the generation of the thrust, $\underline{F}$. The pendulum consists of a point mass $m_2$, attached to a rigid massless rod, which in turn is attached at a point $O$ to the body $B_1$. The length vector of the pendulum is denoted by $\underline{l}$ and the vector from $C_1$ to $O$ is $\underline{r}_o$. Additionally, the angular velocity of the centroidal coordinate system $C$-$xyz$ is denoted by $\underline{\omega}$ and the attitude of the $C$-$xyz$ system is defined by the Euler angles $\Psi$, $\Theta$ and $\Phi$ in a 3-1-3 rotation sequence, as shown in Fig. 4, which are identified as the angles of precession, nutation and proper rotation, respectively.

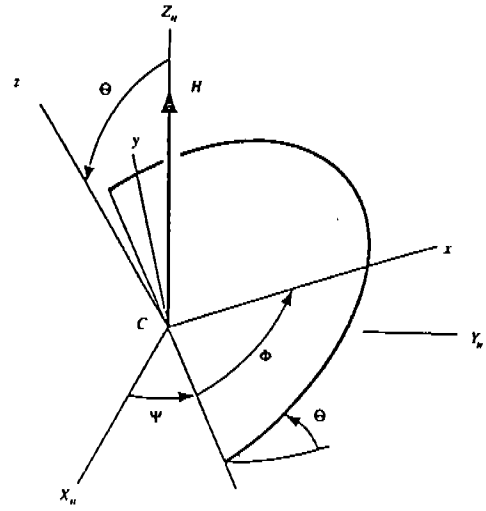


Fig. 4. Orientation of the antenna axes relative to the angular momentum axes.

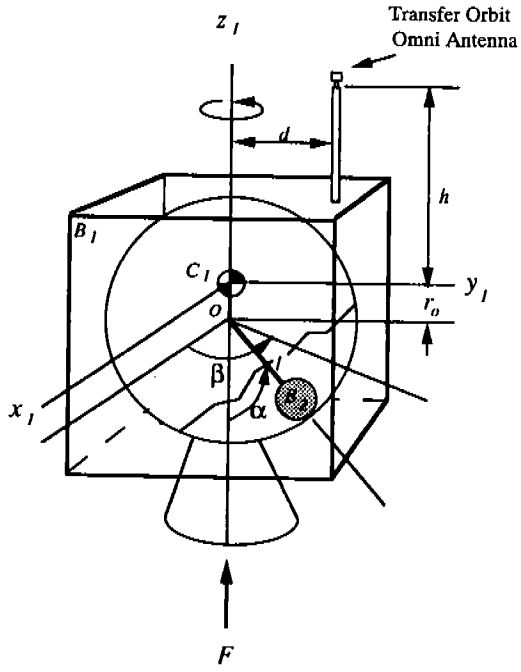


Fig. 3. Two-body satellite model.

## III. MATHEMATICAL MODEL

Equations of motion may be derived for the system of two bodies by using various methods. We have chosen a Newton-projection method in which we write the equations of motion of the system and the equations of relative motion for the pendulum and then eliminate the constraint forces on the pendulum by projection.

Equations governing the motion for the system about its center of mass may be derived by first writing the angular momentum of the system about $C$ in the form

$$\underline{H}=[I]\underline{\omega}+\mu m_1 \underline{r}_p \times [(\underline{\omega}\times \underline{r}_p)+\dot{\underline{r}}_p] \quad (1)$$

where $[I]$ is the centroidal inertia dyadic of the system, $\mu = m_2/(m_1+m_2)$, $\underline{r}_p = \underline{r}_o + \underline{l}$ and $\dot{\underline{r}}_p$

is the time rate of change of $\underline{r}_p$ due to motion of the pendulum relative to $B_1$. By taking components in the $C$-$xyz$ system we can write the following matrix form of $\underline{H}$:

$$\underline{H} = [J]\underline{\omega} + \underline{h} \tag{2}$$

where

$$\underline{h} = \mu m_1 \tilde{\underline{r}}_p \dot{\underline{r}}_p \tag{3}$$

$$[J] = [I] - \mu m_1 \tilde{\underline{r}}_p \tilde{\underline{r}}_p. \tag{4}$$

The tilde over $\underline{r}_p$ denotes the skew-symmetric matrix used to form components of cross-products of vectors. The time derivative of the angular momentum vector $\underline{H}$ gives the matrix equation,

$$\dot{\underline{H}} = \tilde{\underline{H}}\underline{\omega} + \underline{T} \tag{5}$$

where

$$\tilde{\underline{H}} = \begin{bmatrix} 0 & -H_3 & H_2 \\ H_3 & 0 & -H_1 \\ -H_2 & H_1 & 0 \end{bmatrix} \tag{6}$$

$$\underline{\omega} = [J]^{-1}(\dot{\underline{H}} - \underline{h}) \tag{7}$$

$$\underline{T} = (T_1\ T_2\ T_3)^T = -\mu \tilde{\underline{r}}_p \underline{F} \tag{8}$$

$$\underline{F} = (0\ 0\ F_3)^T. \tag{9}$$

An equation for relative motion of the pendulum is more difficult to find. One way to obtain a suitable equation is to write the absolute acceleration of $m_2$, equate it to the force of $m_2$ and cross $\underline{l}$ into both sides of the resulting equation. Let $\underline{a}_c$ be the acceleration of the center of mass. Then, the absolute acceleration of $m_2$ can be expressed as

$$\underline{a}_2 = \underline{a}_c + (1-\mu)[\ddot{\underline{l}} - \tilde{\underline{r}}_p\dot{\underline{\omega}} - 2\dot{\tilde{\underline{l}}}\underline{\omega} - \tilde{\underline{\omega}}\tilde{\underline{r}}_p\underline{\omega}] \tag{10}$$

where

$$\underline{a}_c = \frac{\underline{F}}{m_1 + m_2}, \tag{11}$$

Therefore, the moment equation about the pendulum pivot point $O$ becomes

$$\begin{aligned}\underline{T}_0 &= m_2 \tilde{\underline{l}}\underline{a}_2 \\ &= \mu m_1 l^2 \tilde{\underline{e}}_l \left( \ddot{\underline{e}}_l - \tilde{\underline{e}}_r\dot{\underline{\omega}} + 2\tilde{\omega}\dot{\underline{e}}_l - \tilde{\underline{\omega}}\tilde{\underline{e}}_r\underline{\omega} + \frac{\overline{F}}{m_1 l} \right)\end{aligned} \tag{12}$$

where

$$\underline{e}_1 = \frac{\underline{l}}{l} = \begin{pmatrix} -\sin\alpha\sin\beta \\ \sin\alpha\cos\beta \\ -\cos\alpha \end{pmatrix} \tag{13}$$

$$\underline{e}_r = \frac{\underline{r}_p}{l} = \begin{pmatrix} -\sin\alpha\sin\beta \\ \sin\alpha\cos\beta \\ -\cos\alpha - \dfrac{r_o}{l} \end{pmatrix} \tag{14}$$

and $\underline{T}_o$ is the torque about the pivot point $O$, which may be a liquid friction torque.

Since $\dot{\underline{\omega}}$ appears in (12), instead of $\dot{\underline{H}}$, there is added complication in solving (12) for $\ddot{\alpha}$ and $\ddot{\beta}$. Thus, it is desirable to eliminate $\dot{\omega}$ and $\omega$ from the equations. The necessary substitutions may be carried out fairly easily in a digital computer program. Then, we can find the equations for $\ddot{\alpha}$ and $\ddot{\beta}$ by premultiplying the both sides of (12) by the projection matrix

$$P = \begin{bmatrix} \cos\beta & \sin\beta & 0 \\ -\sin\beta & \cos\beta & 0 \\ 0 & 0 & 0 \end{bmatrix} \tag{15}$$

which reduces the number of equations of motion, 3, to the number of degrees of freedom, 2. The first row of $P$ is a unit vector perpendicular to the plane in which $\alpha$ is measured and the second row is a unit vector orthogonal to the first row.

Since there is no relative motion between the antenna and main body, depointing can be determined by measuring the orientation of the satellite spin axis. The orientation of the satellite body with respect to the angular momentum axes is defined by using the Euler angles $\Psi$, $\Theta$ and $\Phi$ in a 3-1-3 rotation sequence. The well known kinematic equations [8], [9] are

$$\dot{\Psi} = \frac{1}{\sin\Theta}(\omega_1 \sin\Phi + \omega_2 \cos\Phi) \tag{16}$$

$$\dot{\Theta} = \omega_1 \cos\Phi - \omega_2 \sin\Phi \tag{17}$$

$$\dot{\Phi} = \omega_3 - \frac{\cos\Theta}{\sin\Theta}(\omega_1 \sin\Phi + \omega_2 \cos\Phi). \tag{18}$$

By integrating the angular momentum equations and kinematic equations simultaneously, the attitude of the satellite is determined hence the antenna pointing. For graphical presentation of the antenna pointing, the angles of precession and nutation are transformed such that

$$\xi = \Theta \cos\Psi \tag{19}$$

$$\eta = \Theta \sin\Psi. \tag{20}$$

These new coordinates and time axis provide three-dimensional visualization of the satellite pointing instability.

# IV. SIMULATION ANALYSIS FOR VARIOUS SATELLITE BODY CONFIGURATIONS

## 1. Thrust-Free Axisymmetric Rigid Body Model

When the satellite has a single rigid, axisymmetric body configuration in nonthrusting flight mode, (5) becomes a simple Euler's Equation,

$$\dot{\omega}_1 = \left(1 - \frac{1}{\gamma}\right)\omega_2\omega_3 \tag{21}$$

$$\dot{\omega}_2 = -\left(1 - \frac{1}{\gamma}\right)\omega_1\omega_3 \tag{22}$$

$$\dot{\omega}_3 = 0 \tag{23}$$

where $\gamma = I_1/I_3$ and the solutions are easily found in various books [8]-[10].

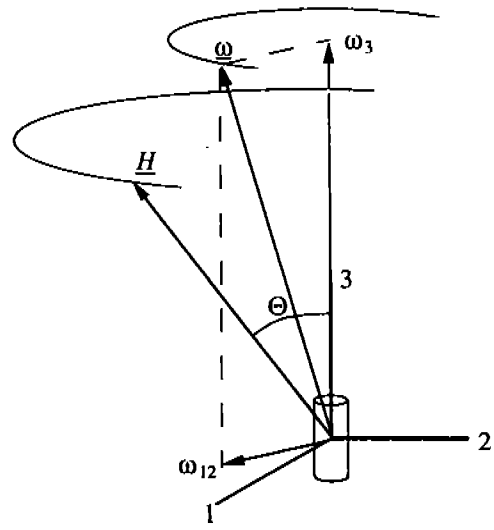


Fig. 5. Angular velocity and angular momentum in the body frame.

Fig. 5 shows the behavior of the $\underline{\omega}$ vector in the body frame. The $\underline{\omega}$ has a constant projection on the symmetry axis, while the projection of the vector on the satellite's plane of symmetry executes a circular motion with angular frequency $(1 - 1/\gamma)$. The $\underline{\omega}$ vector thus describes a cone about the satellite's axis of symmetry. Since there is no applied torque, the

angular momentum vector H is constant with respect to the inertial frame. This is not true when viewed from the body frame. $\underline{H}$ vector also cones about the satellite's symmetry axis with angular frequency $(1-1/\gamma)$. Since the angular momentum vector is fixed in the inertial frame, we can align the angular momentum vector along $CZ_H$ axis, as shown in Fig. 4, in which case the precession rate $\dot{\Psi}$ becomes the angular velocity of the node line and the spin axis about the $CZ_H$ direction. Also, since the nutational motion is bounded, i.e. $\dot{\Theta}=0$, (16)-(18) give

$$\omega_1 = \dot{\Psi}\sin\Theta\sin\Phi \tag{24}$$

$$\omega_2 = \dot{\Psi}\sin\Theta\cos\Phi \tag{25}$$

$$\omega_3 = \dot{\Phi}+\dot{\Psi}\cos\Theta = \text{const.} \tag{26}$$

Differentiating with respect to time once, the angular accelerations are

$$\dot{\omega}_1 = \dot{\Psi}\dot{\Phi}\sin\Theta\cos\Phi \tag{27}$$

$$\dot{\omega}_2 = -\dot{\Psi}\dot{\Phi}\sin\Theta\sin\Phi \tag{28}$$

$$\dot{\omega}_3 = 0. \tag{29}$$

Equating (21) and (27), and using (25) and (26) give

$$\dot{\Psi} = \frac{\dot{\Phi}}{(\gamma-1)\cos\Theta}. \tag{30}$$

This equation states that the null axis of the antenna (or the spin axis of the satellite) rotates about a fixed $CZ_H$ axis ($\underline{H}$ axis) with a speed of $\dot{\Psi}$ proportional to the inertial spin rate $\dot{\Phi}$. If $\gamma > 1$, the satellite is a prolate rigid body, like a slim cylinder, and the precession and spin will occur in the same direction. In this case the precession is called prograde. If $\gamma < 1$, the satellite is an oblate rigid body, like a squat cylinder and the precession is in the opposite sense from the spin, in which the precession is called retrograde. In this latter case the precession rate is greater than the spin rate. As shown in Fig. 6, the precession rate becomes large when $\gamma$ approaches unity and the nutation angle increases. It can be easily proven that the spin rate of the body frame is constant.

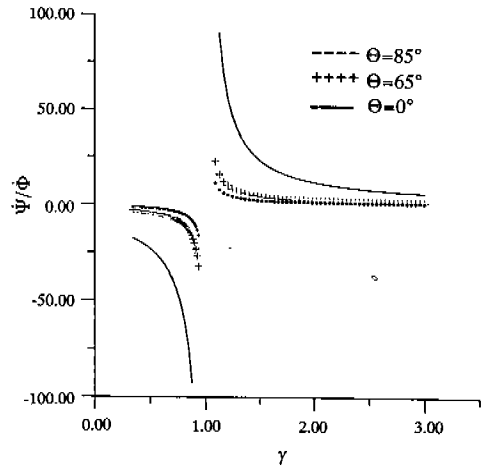


Fig. 6. Variation of the ratio of the precession and spin rates vs. inertia ratio.

## 2. Thrusting Two-Body Spacecraft Model

This model is examined for three particular satellite configurations, the first of which is for an oblate satellite, the second for a symmetric satellite, and the third for a flat satellite. All data used for numerical simulations are same except those of mass properties. As a matter of convenience, it is assumed that the antenna null axis is always aligned with the

spin axis of the satellite and all mass properties are linearly varying with time. Also, the hinge point torque, $\underline{T}_o$, is dropped because it is considered small compared with the thrust-generated-torque. The magnitude of the lateral angular momentum is defined as

$$a=\sqrt{H_1^2+H_2^2}. \tag{31}$$

The basic data used for all cases are as follows:

$$\begin{aligned}
F_3 &= 35000 \text{ N},\\
r_o &= 0 \text{ m},\\
l &= 0.5 \text{ m},\\
d &= 0 \text{ m},\\
h &= 0 \text{ m},\\
H_1(0) &= -0.707 \text{ kg-m}^2/\text{sec},\\
H_2(0) &= 0.707 \text{ kg-m}^2/\text{sec},\\
H_3(0) &= 2\pi n I_3/60 \text{ kg-m}^2/\text{sec},\\
n &= 50 \text{ rpm},\\
\alpha(0) &= \pi/6 \text{ rad},\\
\dot{\alpha}(0) &= 0 \text{ rad/sec},\\
\beta(0) &= \pi/4 \text{ rad},\\
\dot{\beta}(0) &= 0 \text{ rad/sec},\\
\Psi(0) &= 0 \text{ rad},\\
\Theta(0) &= \cos^{-1}\{H_3(0)/H(0)\} \text{ rad},\\
\Phi(0) &= \tan^{-1}\{H_1(0)/H_2(0)\} \text{ rad}.
\end{aligned}$$

A. *Oblate Satellite Model* ($I_1 = I_2 < I_3$)

This case is chosen to investigate the coning behavior of the antenna beam pointing of the satellite which has a squat configuration. Relevant mass properties are given in Table 1. The Case 1.A is for a constant mass model and the Case 1.B for a time-varying mass model.

Table 1. Mass data for oblate rigid body($I_1 = I_2 < I_3$).

| Case | Parameter | at $t=0$ | at $t=50$ | unit |
|---|---|---|---|---|
| 1.A | $m_1$ | 1410 | 1410 | kg |
| | $m_2$ | 0.1 | 0.1 | kg |
| | $I_1$ | 470 | 470 | kg-m$^2$ |
| | $I_2$ | 470 | 470 | kg-m$^2$ |
| | $I_3$ | 560 | 560 | kg-m$^2$ |
| 1.B | $m_1$ | 1410 | 880 | kg |
| | $m_2$ | 0.1 | 1 | kg |
| | $I_1$ | 470 | 410 | kg-m$^2$ |
| | $I_2$ | 470 | 410 | kg-m$^2$ |
| | $I_3$ | 560 | 520 | kg-m$^2$ |

Figs. 7a and b show the time histories of pointing of the antenna beam axes for the corresponding cases, respectively. The vertical axis represents the time axis, which is parallel to the system angular momentum vector direction, and the $\xi\eta$-plane defines the deviation angle of the null axis from the angular momentum vector axis. When the mass properties of the satellite do not vary, wobbling of the antenna null axis is bounded and a beating phenomenon occurs (Fig. 7a). In this case, the beat frequency is the same as that of the angular momentum. When they vary with time, wobbling also grows slowly with time (Fig. 7b). These also can be explained in terms of the system angular momentum. As shown in Fig. 8, the lateral angular momentum is bounded in time-invariant system (Case 1.A) but unbounded in time varying system (Case 1.B).

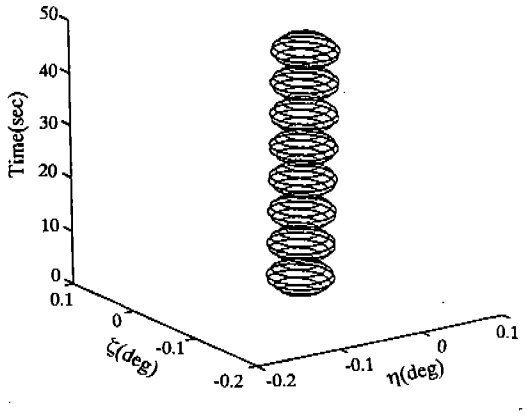


Fig. 7a. Time history of the antenna null-axis pointing for the Case 1.A.

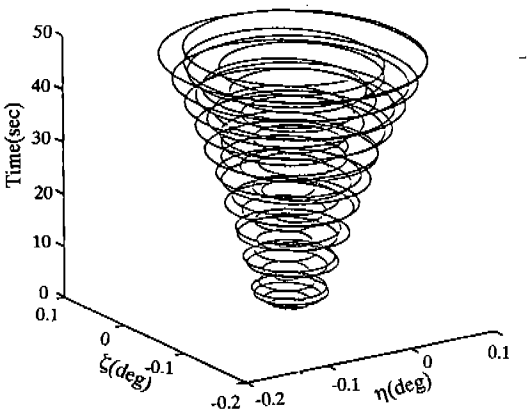


Fig. 7b. Time history of the antenna null-axis pointing for the Case 1.B.

B. *Symmetric Satellite Model* ($I_1 = I_2 = I_3$)

This case is to examine the effect of the symmetric mass moment of inertia on the antenna beam pointing. Relevant mass properties are given in Table 2. The Case 2.A is for a constant mass model and the Case 2.B for a time-varying mass model. Figs. 9a and

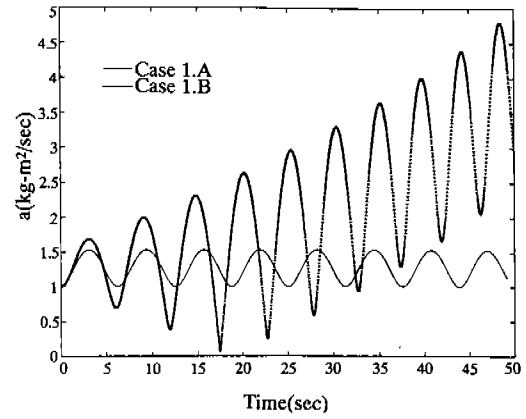


Fig. 8. Time histories of the lateral angular momenta for the Cases 1.A and B.

Table 2. Mass data for symmetric rigid body($I_1 = I_2 = I_3$).

| Case | Parameter | at $t=0$ | at $t=50$ | unit |
|---|---|---|---|---|
| 2.A | $m_1$ | 1410 | 1410 | kg |
| | $m_2$ | 0.1 | 0.1 | kg |
| | $I_1$ | 500 | 500 | kg-m$^2$ |
| | $I_2$ | 500 | 500 | kg-m$^2$ |
| | $I_3$ | 500 | 500 | kg-m$^2$ |
| 2.B | $m_1$ | 1410 | 880 | kg |
| | $m_2$ | 0.1 | 1 | kg |
| | $I_1$ | 500 | 450 | kg-m$^2$ |
| | $I_2$ | 500 | 450 | kg-m$^2$ |
| | $I_3$ | 500 | 450 | kg-m$^2$ |

b show the time histories of the angular displacement of the null axis of the antenna beam for the corresponding cases, respectively. In

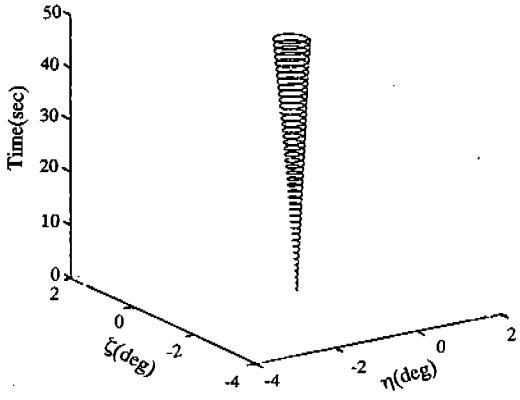


Fig. 9a. Time history of the antenna null-axis pointing for the Case 2.A.

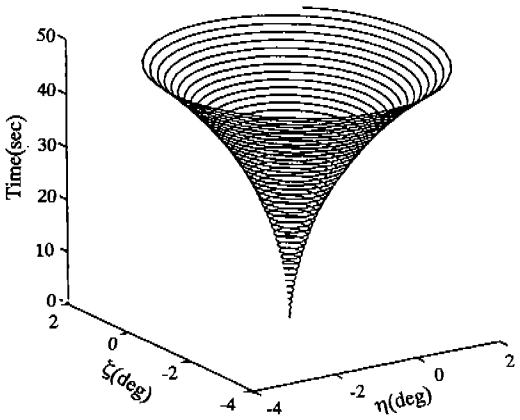


Fig. 9b. Time history of the antenna null-axis pointing for the Case 2.B.

this model, both cases show pointing instability. Even though same parameters are initially used for both cases, the pointing divergence has more rapid growth in the second case than in the first case. Fig. 10 shows the time histories of the corresponding lateral angular momenta.

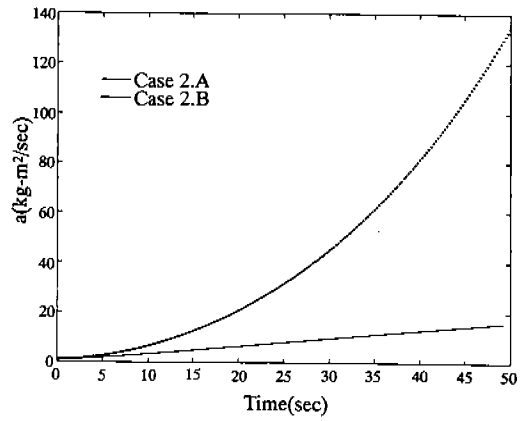


Fig. 10. Time history of the lateral angular momenta for the Cases 2.A and B.

### C. *Prolate Satellite Model* ($I_1 = I_2 > I_3$)

Table 3. Mass data for prolate rigid body($I_1 = I_2 > I_3$).

| Case | Parameter | at $t=0$ | at $t=50$ | unit |
|---|---|---|---|---|
| 3.A | $m_1$ | 1410 | 1410 | kg |
| | $m_2$ | 0.1 | 0.1 | kg |
| | $I_1$ | 515 | 515 | kg-m$^2$ |
| | $I_2$ | 515 | 515 | kg-m$^2$ |
| | $I_3$ | 470 | 470 | kg-m$^2$ |
| 3.B | $m_1$ | 1410 | 880 | kg |
| | $m_2$ | 0.1 | 1 | kg |
| | $I_1$ | 515 | 465 | kg-m$^2$ |
| | $I_2$ | 515 | 465 | kg-m$^2$ |
| | $I_3$ | 470 | 410 | kg-m$^2$ |

In this example the axisymmetric satellite which spins about its minor axis of mass moment of inertia is considered. Data for the mass properties are given in Table 3, in which the

Case 3.A is for a constant mass model and the Case 3.B for a time-varying mass model. Figs. 11a and b are the time histories of the angular displacement of the null axis of the antenna beam for the Cases 3.A and 3.B, respectively. In this model, the first case has a bounded beating motion whose period is the same as that of the angular momentum but the second case has the pointing instability. Fig. 12 shows the time histories of the corresponding lateral angular momenta.

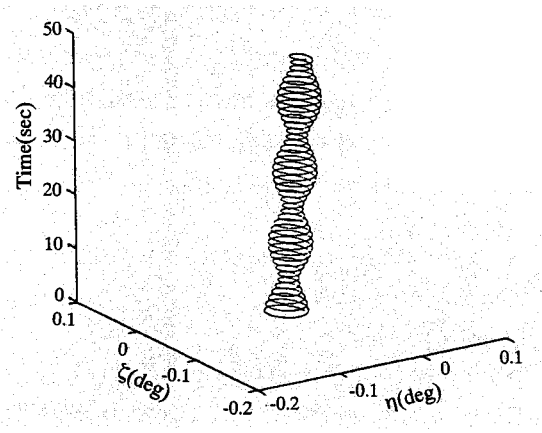


**Fig. 11a.** Time history of the antenna null-axis pointing for the Case 3.A.

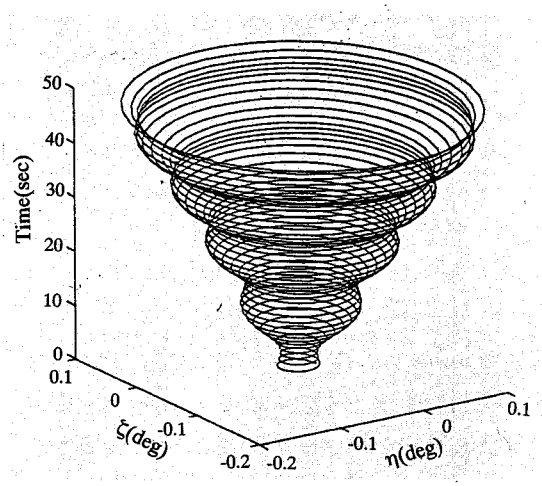


**Fig. 11b.** Time history of the antenna null-axis pointing for the Case 3.B.

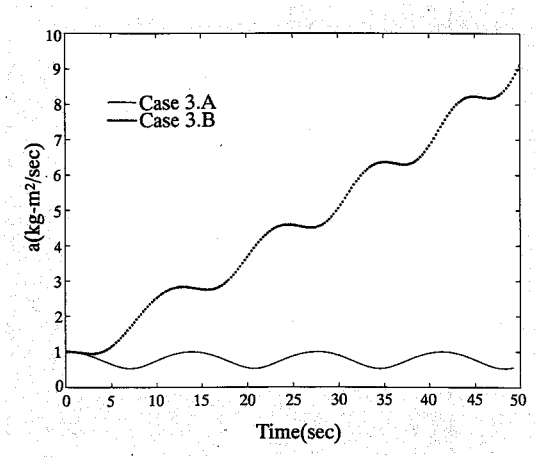


**Fig. 12.** Time histories of the lateral angular momenta for the Cases 3.A and B.

## V. CONCLUSIONS

A mathematical model of a spin-stabilized thrusting satellite subject to the internal mass disturbances has been described and evaluated in terms of its usefulness in explaining the antenna depointing mechanism of such satellites. Equations of motion for two-body satellite system consisting of a main body and a spherical pendulum representing the internal disturbing mass, which can be liquid fuel or liquefied slag of the solid propellant, were derived using Newton's laws of motion. Also, kinematic equations for defining the orienta-

tion of the antenna beam axis of the satellite with respect to the angular momentum vector axis were derived and three basic configurations for the satellite model were tested.

The results of numerical simulations show that, even though the stable main body configuration for the satellite has been chosen, in most cases the pointing instability occurs. As expected, the internal mass disturbance combined with the mass variation and thrusting effects was a main source inducing the antenna pointing instability of a spinning satellite. Among three examined configurations for the satellite, the oblate model has the smallest depointing and the symmetric one the largest. The oblate and prolate models show beating motions whose frequencies are the same as those of the angular momenta.

The dynamical mechanism of the pointing instability of the spinning satellite can be explained as follows: The internal sloshing mass shifts the center of the total mass of the system from the line of the thrust vector and the lateral torque is generated. Therefore, the lateral angular momentum level is increased. Then, the spin axis starts to precess the angular momentum vector and consequently the antenna beam is deviated from its nominal on-axis.

To eliminate or minimize the influences of the internal mass disturbances on the antenna pointing accuracy, mechanical structures such as inner-wall baffles are needed in the liquid storage or the satellite should be designed to have enough gyroscopic stiffness and adequate damping mechanism. Also, using the proposed mathematical models, a satellite engineer may calculate the time change in antenna gain for ground stations initially at boresight or those on the half-power contour as a function of pointing error evaluated for a given satellite model and predict its effect on communications.

## ACKNOWLEDGMENTS

This study was performed as a part of the work accomplished on a research project in which physical and mathematical models for the real-time satellite simulator were developed and tested through the numerical simulation. Fund was provided by the Korea Telecom and Dr. W. J. Jeon acted as the program representative.

## REFERENCES

[1] D. L. Mingori and Y. Yam, "Nutation instability of a spinning spacecraft with internal mass motion and axial thrust," AIAA Paper no. 86-2271, AIAA/AAS Astrodynamics Conference, Williamsburg, VA, Aug. 18-20, 1986.

[2] A. C. Or, "Rotor-pendulum model for the perigee assist module nutation anomaly," *The Journal of Guidance, Control and Dynamics*, vol. 15, no. 2, Mar. 1992, pp. 297-303.

[3] J. E. Cochran, Jr. and J. Y. Kang, "Nonlinear stability analysis of the attitude motion of a spin-stabilized upper stage," AAS Paper 91-190, AAS/AIAA Space flight Mechanics Meeting, Houston, TX, Feb. 11-13, 1991.

[4] J. Y. Kang and J. E. Cochran, Jr., "Further investigation of anomalous attitude motion of a

spin-stabilized upper stage," AAS Paper 91-480, AAS/AIAA Astrodynamics Specialist Conference, Durango, Colorado, Aug. 19-22, 1991.

[5] J. Y. Kang and S. J. Chung, "Resonances in the attitude motion of a spin-stabilized spacecraft," Proceedings of the Asia-Pacific Workshop on Multilateral Cooperation in Space Technology and Applications, Beijing China, Nov. 30 - Dec. 5, 1992, pp. 233-247.

[6] J. Y. Kang, K. K. Shin and J. M. Kim, " The analysis of the attitude motion of a satellite spin-stabilized at apogee phase," Proceedings of the Fall Conference of the Korea Society for Aeronautical & Space Sciences, Seoul Korea, Nov. 14, 1992, pp. 293-301.

[7] N. H. Abramson(ed), "The dynamic behavior of liquids in moving containers with applications to space vehicle technology," *NASA SP-106*, 1966.

[8] W. T. Thomson, *Introduction to Space Dynamics*, New York: Dover Publications Inc., 1986, p. 38, pp. 113-116.

[9] M. H. Kaplan, *Modern Spacecraft Dynamics and Control*, New York: John Wiley & Sons, Inc., 1976, p. 13, pp. 50-57.

[10] P. C. Hughes, *Spacecraft Attitude Dynamics*. New York: John Wiley & Sons, Inc., 1986.

**Ja-Young Kang** received his B.S. degree in M.E. at Chung-Ang University in 1977, M.S. degree at Texas Tech in 1987, and Ph. D. degree in aerospace engineering at Auburn University in 1992.

He worked for the Central International Law & Patent Firm from September 1976 to February 1979 and the Agency for Defense Development from March 1979 to August 1984. He also worked for the Eagle Mark Engineering Co. in 1991. He joined the ETRI as a senior research engineer in June 1992 and is currently in charge of the development of the real time satellite simulator at the Tracking, Telemetry and Command Section of the Satellite Communications Division.

Dr. Kang was awarded an honor for the Outstanding Achievement in Academic Excellence by the Auburn University in 1991 and is a member of AIAA, KOSST, KSASST and KSME. His research area is involved with the dynamics, control and guidance of space flight vehicles.

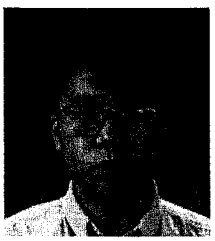

**Kwang-Keun Shin** received his B.S. degree in mechanical engineering from Yonsei University in 1990 and M.S. degree in precision engineering & mechatronics from Korea Advanced Institute of Science and Technology (KAIST) in 1992. He is currently a member of research staff in the Telemetry, Tracking and Command Section at ETRI, and his research area includes spacecraft dynamics, spacecraft control and satellite simulator.